Progress In Electromagnetics Research, PIER 45, 181–199, 2004

MIXED POTENTIAL SPATIAL DOMAIN GREEN'S FUNCTIONS IN FAST COMPUTATIONAL FORM FOR CYLINDRICALLY STRATIFIED MEDIA

J. Sun

Department of Electrical and Computer Engineering
National University of Singapore
Kent Ridge, Singapore 119260

C.-F. Wang

Temasek Laboratories
National University of Singapore
Kent Ridge, Singapore 119260

L.-W. Li † **and M.-S. Leong**

Department of Electrical and Computer Engineering
National University of Singapore
Kent Ridge, Singapore 119260

Abstract—A new procedure for fast computing mixed potential spatial domain Green's functions for cylindrically stratified media is developed in this paper. Based on the fundamental behaviour of electric field Green's functions, spectral domain Green's functions for mixed potential integral equation (MPIE) are formulated by decomposing electric field Green's functions into appropriate forms. The spatial domain mixed potential Green's functions are obtained by using inverse Fourier transform applied to the spectral domain Green's functions. The summations of infinite cylindrical harmonics are accelerated by subtracting a term to resolve the problem of the series' slow convergence and by using the Shank's transform. The Sommerfeld integrals are efficiently evaluated using the discrete complex image method (DCIM) and the generalized pencil of function (GPOF) technique.

† Also with High Performance Computation for Engineered Systems (HPCES) Programme Singapore-MIT Alliance (SMA), Kent Ridge, Singapore 119260

1 Introduction

2 Theory and Formulation

2.1 $\hat{z}$-Oriented Electrical Dipole

2.2 $\hat{\phi}$-Oriented Electrical Dipole

2.3 $\hat{\rho}$-Oriented Electrical Dipole

3 Numerical Results and Discussion

4 Conclusion

References

1. INTRODUCTION

Multilayered cylindrical structures are often used as physical models in many practical applications. Such examples include typical conducting and dielectric cylindrical waveguides, cylindrically-rectangular and wraparound microstrip and patch antennas and their arrays. Numerical modeling of such structures can be efficiently and rigorously performed by employing the method of moments (MoM) although other techniques such as finite element method and finite-difference methods (in both time-domain and frequency-domain) can also be our choices. It is well-known that the MoM procedure for such a problem can be applied either in the spatial domain or in the spectral domain. Although the spectral domain analysis is more suitable and quite efficient for planar structures where the Fourier transform and inverse transform are applied to simplify the problem, the spatial domain analysis is still considered to be more general because it can be easily applied to objects of arbitrary shape and particularly when the Fourier transform cannot be directly applied to formulate and simplify the Green's functions. When the spatial domain Green's functions are used in the numerical MoM procedure, matrix filling is, however, very time consuming sometimes because the Sommerfeld integrals (SIs) are usually involved and numerical evaluation of these integrals is not actually very easy and fast. Therefore, the closed form solution[‡] to the Green's functions becomes necessary. The discrete complex image method (DCIM) for this kind of solutions was proposed in [1–3] for the planarly layered media [4] and then some other important developments of the DCIM were proposed in [5–9]. For cylindrically multilayered media, several important works

[‡] More precisely, the closed form should be referred to as fast computational form. It is because the so-called closed form Green's function is not analytical and it still requires numerical evaluation to obtain the final solution.

appeared in [10–13]. The closed form Green's functions for electric field integral equations (EFIE) in spatial domain are recently reported in [14, 15], where the fast computational solutions to the spatial domain Green's function components due to $\widehat{\boldsymbol{z}}$-, $\widehat{\boldsymbol{\phi}}$- and $\widehat{\boldsymbol{\rho}}$-oriented electrical and magnetic sources embedded in an arbitrary cylindrically multilayered medium are obtained by using the generalized pencil of function (GPOF) method [16].

However, numerical difficulties such as convergence problem arise if we try to obtain spatial domain electric field Green's functions at $\rho = \rho'$, or the source point and the observation point are located on one cylindrical surface. A thorough numerical investigation shows that no reasonable solution is available if we just follow the procedure proposed in [14, 15] without considering the behaviors of Green's functions at $\rho = \rho'$, which is essential and necessary for analyzing cylindrical microstrip structure. To overcome the convergence problem, some researchers computed the mutual impedance of two current sources [17], which are defined as piece-wise sinusoid along the direction of the current and constant along the direction perpendicular to the current. This special choice of current modes is to guarantee the convergence of the spectral domain solution and can be the basis function in many cases. What we want to compute is the Green's function itself and it can be applied to the MoM with different choices of basis functions. The Green's functions usually take two forms. One is the electric field Green's function that is special for EFIE, and the other is mixed potential Green's function that is special for mixed potential integral equation (MPIE). The MPIE is better for analyzing large microstrip structure mounted on layered media, if we can efficiently calculate spatial domain Green's function for the layered media. Some researchers have studied the mixed potential Green's functions for cylindrical microstrip structures [18, 19], where the microstrip is on the surface of one-layer of substrate. However, multiple layered structures are often encountered in practice, such as a radiating patch with one layer of substrate and one layer of superstate. This motivates the present work in the paper. The mixed potential Green's functions and its numerical behavior are investigated in Section 2. In Section 3, some numerical examples of the spatial domain Green's functions are presented for a specific cylindrically multilayered medium. The approximate Green's functions are obtained and compared with the exact solutions obtained by the direct numerical integrals.

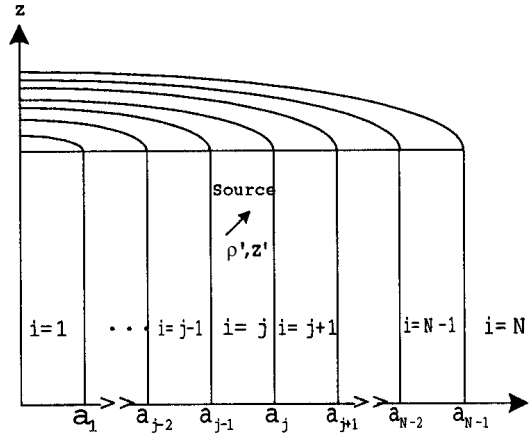

Figure 1. cylindrically multilayered medium.

2. THEORY AND FORMULATION

Consider a cylindrically stratified medium as shown in Fig. 1, in the case of a source point in region j and a field point in region i (where the j and i in the subscript position of the formulation denote the index of the region, while j in other position in the formulation represents the complex number $j = \sqrt{-1}$), the dyadic Green's functions can be written [10] as follows:

$$\begin{aligned}\overline{\boldsymbol{G}}(\boldsymbol{r},\boldsymbol{r}') &= \frac{j}{8\pi}\sum_{m=-\infty}^{\infty}\int_{-\infty}^{\infty} dk_z \frac{1}{(k_j k_{i_\rho})^2}\cdot \overline{\boldsymbol{D}}_{i\mu} \\ &\quad \cdot\overline{\boldsymbol{F}}_n(\rho,\rho') f_n(z,\phi;z',\phi')\cdot \overleftarrow{\overline{\boldsymbol{D}}}_{j\epsilon} - \frac{\hat{\rho}\hat{\rho}}{k_j^2}\delta(\boldsymbol{r}-\boldsymbol{r}') \end{aligned} \tag{1}$$

in which $f_n(z,\phi;z',\phi') = e^{jn(\phi-\phi')+jk_z(z-z')}$ while

$$\begin{aligned}\overline{\boldsymbol{F}}_n(\rho,\rho') &= \begin{bmatrix} f_{11} & f_{12} \\ f_{21} & f_{22} \end{bmatrix} \\ &= \begin{cases} \left[H_n^{(1)}(k_{i_\rho}\rho)\overline{\boldsymbol{I}} + J_n(k_{i_\rho}\rho)\widetilde{\boldsymbol{R}}_{i,i+1}\right]\widetilde{\boldsymbol{A}}, & \rho \geq \rho' \\ \left[J_n(k_{i_\rho}\rho)\overline{\boldsymbol{I}} + H_n^{(1)}(k_{i_\rho}\rho)\widetilde{\boldsymbol{R}}_{i,i-1}\right]\widetilde{\boldsymbol{A}}, & \rho < \rho' \end{cases} \end{aligned} \tag{2}$$

and $\widetilde{\boldsymbol{A}}$ denotes a 2×2 amplitude matrix for the standing and outgoing waves, defined

$$\widetilde{\boldsymbol{A}} = \widetilde{\boldsymbol{M}}_i \cdot \widetilde{\boldsymbol{T}}_{ji} \cdot \widetilde{\boldsymbol{M}}_j \cdot \overline{\boldsymbol{B}}. \tag{3}$$

In Eq. (3), $\widetilde{\boldsymbol{M}}_i$ and $\widetilde{\boldsymbol{M}}_j$ represent the generalized multi-reflection matrices in layer i and layer j, respectively, $\widetilde{\boldsymbol{T}}_{ji}$ denotes the generalized transmission matrix from layer j to layer i, as defined in [10], and matrix $\overline{\boldsymbol{B}}$ is defined by

$$\overline{\boldsymbol{B}} = \begin{cases} \left[J_n(k_{j_\rho}\rho')\overline{\boldsymbol{I}} + H_n^{(1)}(k_{j_\rho}\rho')\widetilde{\boldsymbol{R}}_{j,j-1}\right], & \rho \geq \rho' \\ \left[H_n^{(1)}(k_{j_\rho}\rho')\overline{\boldsymbol{I}} + J_n(k_{j_\rho}\rho')\widetilde{\boldsymbol{R}}_{j,j+1}\right], & \rho < \rho' \end{cases} \tag{4}$$

where

$$\overline{\boldsymbol{D}}_{i\mu} = [\nabla \times \nabla \times \hat{z}, j\omega\mu_i \nabla \times \hat{z}]$$

and

$$\overleftarrow{\overline{\boldsymbol{D}}}_{j\epsilon} = \left[\nabla' \times \nabla' \times \hat{z}', -j\omega\epsilon_j \nabla \times \hat{z}'\right]^t \cdot \hat{\alpha}$$

operate on the primed coordinates to its left, $\hat{\alpha}$ denotes the direction of the source, $\widetilde{\boldsymbol{R}}_{j,j-1}$ and $\widetilde{\boldsymbol{R}}_{j,j+1}$ stand for the reflection matrices. Based on above expressions, we can obtain the spectral Green's functions subsequently [15].

2.1. $\hat{z}$-Oriented Electrical Dipole

$$\widetilde{G}_{zz}^{E_n} = -\frac{1}{8\pi\epsilon_j\omega} \cdot k_{j\rho}^2 f_{11} \tag{5a}$$

$$\widetilde{G}_{\phi z}^{E_n} = \frac{1}{8\pi\epsilon_j\omega k_{i\rho}^2} \cdot k_{j\rho}^2 \left(-\frac{k_z n}{\rho} f_{11} - j\omega\mu_i \frac{\partial f_{21}}{\partial \rho}\right) \tag{5b}$$

$$\widetilde{G}_{\rho z}^{E_n} = \frac{1}{8\pi\epsilon_j\omega k_{i\rho}^2} \cdot k_{j\rho}^2 \left(-jk_z \frac{\partial f_{11}}{\partial \rho} + \frac{n\omega\mu_i}{\rho} f_{21}\right). \tag{5c}$$

2.2. $\hat{\phi}$-Oriented Electrical Dipole

$$\widetilde{G}_{z\phi}^{E_n} = -\frac{1}{8\pi\epsilon_j\omega} \cdot \left(j\omega\epsilon_j \frac{\partial f_{12}}{\partial \rho'} + \frac{k_z n}{\rho'} f_{11}\right) \tag{6a}$$

$$\begin{aligned} \widetilde{G}_{\phi\phi}^{E_n} = & -\frac{1}{8\pi\epsilon_j\omega k_{i\rho}^2} \cdot \left[\frac{k_z n}{\rho'}\left(\frac{k_z n}{\rho} f_{11} + j\omega\mu_i \frac{\partial f_{21}}{\partial \rho}\right)\right. \\ & \left. - j\omega\epsilon_j \left(\frac{k_z n}{\rho} \frac{\partial f_{12}}{\partial \rho'} + j\omega\mu_i \frac{\partial^2 f_{22}}{\partial\rho\partial\rho'}\right)\right] \end{aligned} \tag{6b}$$

$$\begin{aligned} \widetilde{G}_{\rho\phi}^{E_n} = & -\frac{1}{8\pi\epsilon_j\omega} \cdot \left[jk_z \left(j\omega\epsilon_j \frac{\partial^2 f_{12}}{\partial\rho\partial\rho'} - \frac{k_z n}{\rho'} \frac{\partial f_{11}}{\partial \rho}\right)\right. \\ & \left. - \frac{n\omega\mu_i}{\rho}\left(j\omega\epsilon_j \frac{\partial f_{22}}{\partial \rho'} - \frac{k_z n}{\rho'} f_{21}\right)\right]. \end{aligned} \tag{6c}$$

2.3. $\hat{\rho}$-Oriented Electrical Dipole

$$\widetilde{G}^{E_n}_{z\rho} = \frac{1}{8\pi\epsilon_j\omega}\cdot\left(jk_z\frac{\partial f_{11}}{\partial\rho'}+\frac{n\omega\epsilon_j}{\rho'}f_{12}\right) \tag{7a}$$

$$\widetilde{G}^{E_n}_{\phi\rho} = \frac{1}{8\pi\epsilon_j\omega k^2_{i\rho}}\cdot\left[\frac{k_z n}{\rho}\left(jk_z\frac{\partial f_{11}}{\partial\rho'}+\frac{n\omega\epsilon_j}{\rho'}f_{12}\right)+j\omega\mu_j\left(jk_z\frac{\partial^2 f_{21}}{\partial\rho\partial\rho'}+\frac{n\omega\epsilon_j}{\rho'}\frac{\partial f_{22}}{\partial\rho}\right)\right] \tag{7b}$$

$$\widetilde{G}^{E_n}_{\rho\rho} = \frac{1}{8\pi\epsilon_j\omega k^2_{i\rho}}\cdot\left[\frac{jk_z}{\rho}\left(-jk_z\frac{\partial^2 f_{11}}{\partial\rho\partial\rho'}-\frac{n\omega\epsilon_j}{\rho'}\frac{\partial f_{12}}{\partial\rho}\right)+\frac{\omega n\mu_i}{\rho}\left(jk_z\frac{\partial f_{21}}{\partial\rho'}+\frac{n\omega\epsilon_j}{\rho'}f_{22}\right)\right]. \tag{7c}$$

In this paper, we assume the current to be $J_\rho = 0$. The two dimensional consideration comes from the fact that most practical circuits or antennas are conformed to the multilayered cylindrical structure. The mixed potential Green's function will be derived from the electric field Green's functions in (5)–(7). The electric field due to the current can be expressed in a mixed potential form as follows:

$$\boldsymbol{E} = -j\omega\boldsymbol{A}-\nabla\phi \tag{8}$$

where

$$\boldsymbol{A} = \iint_s \overline{\boldsymbol{G}}_A\cdot\boldsymbol{J}(\boldsymbol{r}')ds'. \tag{9}$$

The electric scalar potential is related the vector potential by Lorentz gauge. To deduce the scalar potential Green's function, one must transform the divergence operator to act on the current density. A general form of ϕ is postulated [20] as

$$\phi = \iint_s \nabla'\cdot\overline{\boldsymbol{G}}_\phi\cdot\boldsymbol{J}(\boldsymbol{r}')ds'. \tag{10}$$

Assume that $\widetilde{\overline{\boldsymbol{G}}}_E$, $\widetilde{\overline{\boldsymbol{G}}}_A$, $\widetilde{\overline{\boldsymbol{G}}}_\phi$ are the spectral domain counterparts of $\overline{\boldsymbol{G}}_E$, $\overline{\boldsymbol{G}}_A$, $\overline{\boldsymbol{G}}_\phi$, respectively. Then, we have

$$\widetilde{\overline{\boldsymbol{G}}}_E = -j\omega\widetilde{\overline{\boldsymbol{G}}}_A-\nabla\nabla'\cdot(\widetilde{\overline{\boldsymbol{G}}}_\phi) \tag{11}$$

where

$$\widetilde{\overline{\boldsymbol{G}}}_E = \begin{bmatrix}\widetilde{G}^E_{\rho\rho} & \widetilde{G}^E_{\rho\phi} & \widetilde{G}^E_{\rho z}\\ \widetilde{G}^E_{\phi\rho} & \widetilde{G}^E_{\phi\phi} & \widetilde{G}^E_{\phi z}\\ \widetilde{G}^E_{z\rho} & \widetilde{G}^E_{z\phi} & \widetilde{G}^E_{zz}\end{bmatrix} \tag{12a}$$

$$\overline{\overline{\boldsymbol{G}}}_A = \begin{bmatrix} \widetilde{G}^A_{\rho\rho} & \widetilde{G}^A_{\rho\phi} & \widetilde{G}^A_{\rho z} \\ \widetilde{G}^A_{\phi\rho} & \widetilde{G}^A_{\phi\phi} & \widetilde{G}^A_{\phi z} \\ \widetilde{G}^A_{z\rho} & \widetilde{G}^A_{z\phi} & \widetilde{G}^A_{zz} \end{bmatrix} \tag{12b}$$

$$\overline{\overline{\boldsymbol{G}}}_\phi = \begin{bmatrix} \widetilde{G}^\phi_{\rho\rho} & 0 & 0 \\ 0 & \widetilde{G}^\phi_{\phi\phi} & 0 \\ 0 & 0 & \widetilde{G}^\phi_{zz} \end{bmatrix}. \tag{12c}$$

By using dyadic identities, $\nabla\nabla' \cdot (\overline{\overline{\boldsymbol{G}}}_\phi)$ can be expanded as

$$\begin{aligned} \nabla\nabla' \cdot (\overline{\overline{\boldsymbol{G}}}_\phi) = {} & \widehat{\boldsymbol{\rho}} \left[\left(\frac{1}{\rho'} \frac{\partial^2 \widetilde{G}^\phi_{\rho\rho}}{\partial \rho} + \frac{\partial^2 \widetilde{G}^\phi_{\rho\rho}}{\partial \rho \partial \rho'} - \frac{1}{\rho'} \frac{\partial^2 \widetilde{G}^\phi_{\phi\phi}}{\partial \rho} \right) \widehat{\boldsymbol{\rho}} \right. \\ & \left. + \frac{1}{\rho'} \frac{\partial^2 \widetilde{G}^\phi_{\phi\phi}}{\partial \rho \partial \phi'} \widehat{\boldsymbol{\phi}} + \frac{\partial^2 \widetilde{G}^\phi_{zz}}{\partial \rho \partial z'} \widehat{\boldsymbol{z}} \right] \\ & + \frac{1}{\rho} \widehat{\boldsymbol{\phi}} \left[\left(\frac{1}{\rho'} \frac{\partial \widetilde{G}^\phi_{\rho\rho}}{\partial \phi} + \frac{\partial^2 \widetilde{G}^\phi_{\rho\rho}}{\partial \phi \partial \rho'} - \frac{1}{\rho'} \frac{\partial \widetilde{G}^\phi_{\phi\phi}}{\partial \phi} - \frac{1}{\rho'} \frac{\partial \widetilde{G}^\phi_{\phi\phi}}{\partial \phi'} \right) \widehat{\boldsymbol{\rho}} \right. \\ & + \left(\frac{1}{\rho'} \frac{\partial^2 \widetilde{G}^\phi_{\phi\phi}}{\partial \phi \partial \phi'} + \frac{\widetilde{G}^\phi_{\rho\rho}}{\rho'} + \frac{\partial \widetilde{G}^\phi_{\rho\rho}}{\partial \rho'} - \frac{1}{\rho'} \widetilde{G}^\phi_{\phi\phi} \right) \widehat{\boldsymbol{\phi}} + \frac{\partial^2 \widetilde{G}^\phi_{zz}}{\partial \phi \partial z'} \widehat{\boldsymbol{z}} \left. \right] \\ & + \widehat{\boldsymbol{z}} \left[\left(\frac{\partial^2 \widetilde{G}^\phi_{\rho\rho}}{\partial z \partial \rho'} + \frac{1}{\rho'} \frac{\widetilde{G}^\phi_{\rho\rho}}{\partial z} - \frac{1}{\rho'} \frac{\widetilde{G}^\phi_{\phi\phi}}{\partial z} \right) \widehat{\boldsymbol{\rho}} \right. \\ & \left. + \frac{1}{\rho'} \frac{\partial^2 \widetilde{G}^\phi_{\phi\phi}}{\partial \rho \partial \phi'} \widehat{\boldsymbol{\phi}} + \frac{\partial^2 \widetilde{G}^\phi_{zz}}{\partial z \partial z'} \widehat{\boldsymbol{z}} \right]. \end{aligned} \tag{13}$$

From Eqs. (8)–(13), the tangential electric field components can be written as follows:

$$\begin{aligned} \begin{bmatrix} \widetilde{\boldsymbol{E}}_\phi \\ \widetilde{\boldsymbol{E}}_z \end{bmatrix} = & \begin{bmatrix} \widetilde{G}^E_{\phi\rho} & \widetilde{G}^E_{\phi\phi} & \widetilde{G}^E_{\phi z} \\ \widetilde{G}^E_{z\rho} & \widetilde{G}^E_{z\phi} & \widetilde{G}^E_{zz} \end{bmatrix} \cdot \begin{bmatrix} J_\rho \\ J_\phi \\ J_z \end{bmatrix} \\ = & -j\omega \begin{bmatrix} \widetilde{G}^A_{\phi\rho} & \widetilde{G}^A_{\phi\phi} & \widetilde{G}^A_{\phi z} \\ \widetilde{G}^A_{z\rho} & \widetilde{G}^A_{z\phi} & \widetilde{G}^A_{zz} \end{bmatrix} \cdot \begin{bmatrix} J_\rho \\ J_\phi \\ J_z \end{bmatrix} - [\nabla\nabla' \cdot (\overline{\overline{\boldsymbol{G}}}_\phi)]_t \cdot \begin{bmatrix} J_\rho \\ J_\phi \\ J_z \end{bmatrix} \end{aligned} \tag{14}$$

in which $\nabla\nabla'\cdot(\overline{\overline{\boldsymbol{G}}}_\phi)_t$ denotes the tangential component of $\nabla\nabla'\cdot(\overline{\overline{\boldsymbol{G}}}_\phi)$, and is given by

$$\begin{aligned}\nabla\nabla'\cdot(\overline{\overline{\boldsymbol{G}}}_\phi)_t \;=\; & \frac{1}{\rho}\widehat{\boldsymbol{\phi}}\left[\left(\frac{1}{\rho'}\frac{\partial\widetilde{G}^\phi_{\rho\rho}}{\partial\phi}+\frac{\partial^2\widetilde{G}^\phi_{\rho\rho}}{\partial\phi\partial\rho'}-\frac{1}{\rho'}\frac{\partial\widetilde{G}^\phi_{\phi\phi}}{\partial\phi}-\frac{1}{\rho'}\frac{\partial\widetilde{G}^\phi_{\phi\phi}}{\partial\phi'}\right)\widehat{\boldsymbol{\rho}}\right.\\ & +\left(\frac{1}{\rho'}\frac{\partial^2\widetilde{G}^\phi_{\phi\phi}}{\partial\phi\partial\phi'}+\frac{\widetilde{G}^\phi_{\rho\rho}}{\rho'}+\frac{\partial\widetilde{G}^\phi_{\rho\rho}}{\partial\rho'}-\frac{1}{\rho'}\widetilde{G}^\phi_{\phi\phi}\right)\widehat{\boldsymbol{\phi}}\\ & \left.+\frac{\partial^2\widetilde{G}^\phi_{zz}}{\partial\phi\partial z'}\widehat{\boldsymbol{z}}\right]+\widehat{\boldsymbol{z}}\left[\left(\frac{\partial^2\widetilde{G}^\phi_{\rho\rho}}{\partial z\partial\rho'}+\frac{1}{\rho'}\frac{\widetilde{G}^\phi_{\rho\rho}}{\partial z}-\frac{1}{\rho'}\frac{\widetilde{G}^\phi_{\phi\phi}}{\partial z}\right)\widehat{\boldsymbol{\rho}}\right.\\ & \left.+\frac{1}{\rho'}\frac{\partial^2\widetilde{G}^\phi_{\phi\phi}}{\partial z\partial\phi'}\widehat{\boldsymbol{\phi}}+\frac{\partial^2\widetilde{G}^\phi_{zz}}{\partial z\partial z'}\widehat{\boldsymbol{z}}\right]. \end{aligned}\tag{15}$$

If the patch was conformed to a cylinder, it is reasonable to postulate that current component $J_\rho = 0$. Without losing of any generality, we assume that $\widetilde{G}^\phi_{\rho\rho}=0$ and, $\widetilde{G}^\phi_{\phi\phi}=\widetilde{G}^\phi_{zz}=\widetilde{G}^\phi$.

Therefore, (15) and (14) can be further reduced to

$$\begin{aligned}\begin{bmatrix}\widetilde{\boldsymbol{E}}_\phi\\ \widetilde{\boldsymbol{E}}_z\end{bmatrix}_{J_\rho=0} =& \begin{bmatrix}\widetilde{G}^E_{\phi\phi} & \widetilde{G}^E_{\phi z}\\ \widetilde{G}^E_{z\phi} & \widetilde{G}^E_{zz}\end{bmatrix}\cdot\begin{bmatrix}J_\phi\\ J_z\end{bmatrix}\\ =& -j\omega\begin{bmatrix}\widetilde{G}^A_{\phi\phi} & \widetilde{G}^A_{\phi z}\\ \widetilde{G}^A_{z\phi} & \widetilde{G}^A_{zz}\end{bmatrix}\cdot\begin{bmatrix}J_\phi\\ J_z\end{bmatrix}-\nabla\nabla'\cdot(\overline{\overline{\boldsymbol{G}}}_\phi)_t\cdot\begin{bmatrix}J_\phi\\ J_z\end{bmatrix}\end{aligned}\tag{16}$$

where

$$\begin{aligned}\nabla\nabla'\cdot(\overline{\overline{\boldsymbol{G}}}_\phi)_t \;=\; & \frac{1}{\rho}\widehat{\boldsymbol{\phi}}\left[\left(\frac{1}{\rho'}\frac{\partial^2\widetilde{G}^\phi}{\partial\phi\partial\phi'}-\frac{1}{\rho'}\widetilde{G}^\phi\right)\widehat{\boldsymbol{\phi}}+\frac{\partial^2\widetilde{G}^\phi}{\partial\phi\partial z'}\widehat{\boldsymbol{z}}\right]\\ & +\widehat{\boldsymbol{z}}\left(\frac{1}{\rho'}\frac{\partial^2\widetilde{G}^\phi}{\partial z\partial\phi'}\widehat{\boldsymbol{\phi}}+\frac{\partial^2\widetilde{G}^\phi}{\partial z\partial z'}\widehat{\boldsymbol{z}}\right).\end{aligned}\tag{17}$$

By comparing it with $\widetilde{G}^{E_n}_{zz}$, $\widetilde{G}^{E_n}_{z\phi}$, $\widetilde{G}^{E_n}_{\phi z}$, $\widetilde{G}^{E_n}_{\phi\phi}$ in Eqs. (5)–(7) and from Eq. (16), it can be obtained that

$$\widetilde{G}^{E_n}_{zz} \;=\; -j\omega\widetilde{G}^A_{zz}-k_z^2\widetilde{G}^\phi \tag{18a}$$

$$\widetilde{G}^{E_n}_{z\phi} \;=\; -j\omega\widetilde{G}^A_{z\phi}-\frac{k_z n}{\rho}\widetilde{G}^\phi \tag{18b}$$

$$\widetilde{G}_{\phi z}^{E_n} = -j\omega\widetilde{G}_{\phi z}^{A} - \frac{k_z n}{\rho'}\widetilde{G}^{\phi} \tag{18c}$$

$$\widetilde{G}_{\phi\phi}^{E_n} = -j\omega\widetilde{G}_{\phi\phi}^{A} - \frac{n^2-1}{\rho\rho'}\widetilde{G}^{\phi}. \tag{18d}$$

Since $\widetilde{G}_{z\phi}^{E_n} = \widetilde{G}_{\phi z}^{E_n}$ when $\rho = \rho'$, and by letting $\widetilde{G}_{z\phi}^{A} = \widetilde{G}_{\phi z}^{A} = 0$, then (18b) and (18c) can be used to uniquely determine $\widetilde{G}^{\phi}$ as follows:

$$\widetilde{G}^{\phi} = -\frac{1}{8\pi\epsilon_j\omega}\cdot\left(f_{11} + \frac{j\rho\omega\mu_i}{k_z n}\frac{\partial f_{21}}{\partial\rho}\right). \tag{19}$$

Substituting $\widetilde{G}^{\phi}$ into (18a) and (18d), and solving for $\widetilde{G}_{zz}^{A}$ and $\widetilde{G}_{\phi\phi}^{A}$, then we have

$$\widetilde{G}_{zz}^{A} = -\frac{j}{8\pi\epsilon_j\omega^2}\cdot\left(k_i^2 f_{11} + \frac{j\rho\omega\mu_i k_z}{n}\frac{\partial f_{21}}{\partial\rho}\right). \tag{20a}$$

$$\begin{aligned}\widetilde{G}_{\phi\phi}^{A} = &-\frac{j}{8\pi\epsilon_j\omega^2 k_{i\rho}^2}\cdot\left\{k_j^2\left(\frac{n^2 f_{11}}{\rho\rho'} + \frac{j\omega\mu_i n}{\rho' k_z}\frac{\partial f_{21}}{\partial\rho}\right)\right.\\ &\left.- j\omega\epsilon_j\left(\frac{k_z n}{\rho}\frac{\partial f_{12}}{\partial\rho'} + j\omega\mu_i\frac{\partial^2 f_{22}}{\partial\rho\partial\rho'}\right)\right\}\\ &+\frac{1}{8\pi\epsilon_j\omega^2}\cdot\left(f_{11} + \frac{j\rho\omega\mu_i}{k_z n}\frac{\partial f_{21}}{\partial\rho}\right).\end{aligned} \tag{20b}$$

The inverse Fourier transform can be written in a general form as follows:

$$G(\boldsymbol{r},\boldsymbol{r}') = \sum_{n=-\infty}^{\infty}\int_{-\infty}^{\infty} e^{jn(\phi-\phi')+jk_z(z-z')}\widetilde{G}(n,k_z)dk_z \tag{21}$$

where $\widetilde{G}(n,k_z)$ denotes dyadic components or dyads in (19), (20a) and (20b).

This type of Sommerfeld integrals is very time consuming to evaluate, if a direct numerical integration is utilized. But it can be efficiently evaluated using the DCIM and the GPOF technique. In order to do so, an infinite number of cylindrical harmonic has to be summed up carefully by taking into the account the slow convergence behavior of the series of cylindrical harmonics. This process is much different from that either using MPIE for the planar layered media or EFIE for multilayered cylindrical media when $\rho \neq \rho'$.

In this connection, we will discuss in detail how to truncate efficiently the summation of infinite number of cylindrical harmonics.

Numerical investigation shows that the condition $\rho = \rho'$ will lead the summation of cylindrical harmonics in (19), (20a) and (20b) to be slowly convergent or even divergent. For further convenient analysis, the expression of f_{11} is given as an example:

$$\begin{aligned} f_{11} &= \left\{\left[H_n^{(1)}(k_{i_\rho}\rho) + J_n(k_{i_\rho}\rho)R_{i,i+1}(1,1)\right]M_i(1,1)\right. \\ &\quad \left.+J_n(k_{i_\rho}\rho)R_{i,i+1}(1,2)M_i(2,1)\right\} \\ &\quad \cdot\left[J_n(k_{i_\rho}\rho') + H_n^{(1)}(k_{i_\rho}\rho')R_{i,i-1}(1,1)\right] \\ &\quad + \left\{\left[H_n^{(1)}(k_{i_\rho}\rho) + J_n(k_{i_\rho}\rho)R_{i,i+1}(1,1)\right]M_i(1,2)\right. \\ &\quad \left.+J_n(k_{i_\rho}\rho)R_{i,i+1}(1,2)M_i(2,2)\right\}\left[H_n^{(1)}(k_{i_\rho}\rho')R_{i,i-1}(1,1)\right] \quad (22) \end{aligned}$$

where $R_{i,i+1}(p,q)$, $R_{i,i-1}(p,q)$, and $M_i(p,q)$ with ($p = 1,2$; and $q = 1,2$) are elements of matrix $\widetilde{\boldsymbol{R}}_{i,i+1}$, $\widetilde{\boldsymbol{R}}_{i,i-1}$ and $\widetilde{\boldsymbol{M}}_i$, respectively. Numerical analysis shows that the real parts of $M_1(1,1)$ and $M_1(2,2)$ approach 1, and the imaginary parts of $M_1(1,1)$ and $M_1(2,2)$ approach 0 when n or k_z becomes large. And both the real part and imaginary part of $M_1(1,2)$ and $M_1(2,1)$ approach 0 when n or k_z becomes large. The physical significance is that TE and TM modes are weakly coupled each other when n or k_z becomes large. In other words, f_{11} implicitly contains a component $[H_n^{(1)}(k_{i_\rho}\rho)J_n(k_{i_\rho}\rho')]$. Consider the summation of harmonics as follows:

$$S(m) = \sum_{n=-m}^{m} H_n^{(1)}(k_{i_\rho}\rho)J_n(k_{i_\rho}\rho')e^{jn(\phi-\phi')}. \quad (23)$$

The property of convergence with respect to total number of summation m is shown in Fig. 2 for a set of specific value. It can be seen that $S(m)$ is slowly convergent with index m. Fortunately, the following additional theorem obviates the brutal force evaluation of $S(m)$:

$$H_0^{(1)}(k_{i\rho}|\boldsymbol{\rho} - \boldsymbol{\rho}'|) = \sum_{n=-\infty}^{\infty} H_n^{(1)}(k_{i_\rho}\rho)J_n(k_{i_\rho}\rho')e^{jn(\phi-\phi')}. \quad (24)$$

This fact reminds us to rearrange f_{11} as follows,

$$\begin{aligned} f_{11} &= \left\{\left[H_n^{(1)}(k_{i_\rho}\rho) + J_n(k_{i_\rho}\rho)R_{i,i+1}(1,1)\right]M_i(1,1)\right. \\ &\quad \left.+J_n(k_{i_\rho}\rho)R_{i,i+1}(1,2)M_i(2,1)\right\} \end{aligned}$$

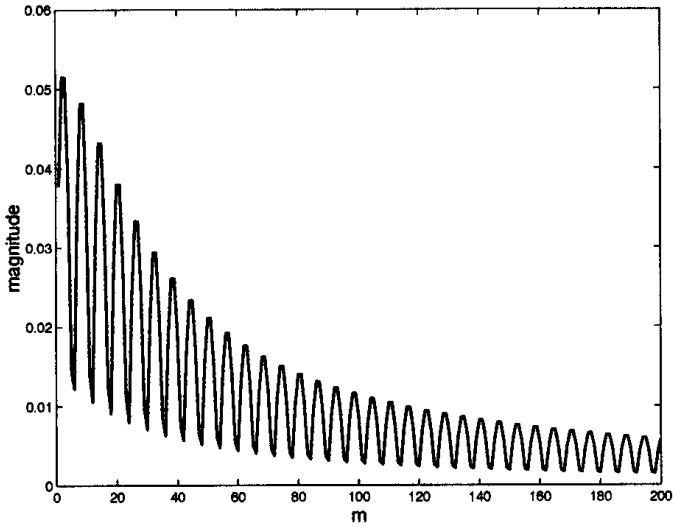

Figure 2. Slowly convergent behavior of summation $|S(m)|$ when $\rho = \rho' = 0.051$, $\phi - \phi' = \pi/6$, $\epsilon_{r_i} = 2.3$, $\mu_{r_i} = 1$, $f = 6.8\,\text{GHz}$, $k_z = 500$ which is one sampling point located on the Sommerfeld integral path.

$$
\begin{aligned}
&\cdot \left[J_n(k_{i_\rho}\rho') + H_n^{(1)}(k_{i_\rho}\rho')R_{i,i-1}(1,1)\right] \\
&+ \left\{\left[H_n^{(1)}(k_{i_\rho}\rho) + J_n(k_{i_\rho}\rho)R_{i,i+1}(1,1)\right] M_i(1,2)\right. \\
&\left.+J_n(k_{i_\rho}\rho)R_{i,i+1}(1,2)M_i(2,2)\right\}\left[H_n^{(1)}(k_{i_\rho}\rho')R_{i,i-1}(1,1)\right] \\
&-H_n^{(1)}(k_{i_\rho}\rho)J_n(k_{i_\rho}\rho') + H_n^{(1)}(k_{i_\rho}\rho)J_n(k_{i_\rho}\rho') \\
= \;& f'_{11} + H_n^{(1)}(k_{i_\rho}\rho)J_n(k_{i_\rho}\rho') \qquad (25a)
\end{aligned}
$$

Numerical investigation shows that $\sum f'_{11}e^{jn(\phi-\phi')}$ converges much faster than $\sum f_{11}e^{jn(\phi-\phi')}$ when $\rho = \rho'$. The similar arrangement can be applied to f_{22} while we keep f_{12} and f_{21} as their original forms, since they do not implicitly contain $[H_n^{(1)}(k_{i_\rho}\rho)J_n(k_{i_\rho}\rho')]$ as f_{11} and f_{22}. For clear understanding and complete, the expressions of f_{12}, f_{21} and f_{22} are listed below:

$$
\begin{aligned}
f_{12} \;=\; & \left\{\left[H_n^{(1)}(k_{i_\rho}\rho) + J_n(k_{i_\rho}\rho)R_{i,i+1}(1,1)\right] M_i(1,1)\right. \\
& \left.+J_n(k_{i_\rho}\rho)R_{i,i+1}(1,2)M_i(2,1)\right\}H_n^{(1)}(k_{i_\rho}\rho')R_{i,i-1}(1,2)
\end{aligned}
$$

$$
\begin{aligned}
&+\left\{\left[H_n^{(1)}(k_{i_\rho}\rho)+J_n(k_{i_\rho}\rho)R_{i,i+1}(1,1)\right]M_i(1,2)\right.\\
&\left.+J_n(k_{i_\rho}\rho)R_{i,i+1}(1,2)M_i(2,2)\right\}\\
&\cdot\left[J_n(k_{i_\rho}\rho')+H_n^{(1)}(k_{i_\rho}\rho')R_{i,i-1}(2,2)\right] \qquad (25b)\\
f_{21} &= \left\{J_n(k_{i_\rho}\rho)R_{i,i+1}(2,1)M_i(1,1)\right.\\
&\left.+\left[H_n^{(1)}(k_{i_\rho}\rho)+J_n(k_{i_\rho}\rho)R_{i,i+1}(2,2)\right]M_i(2,1)\right\}\\
&\cdot\left[J_n(k_{i_\rho}\rho')+H_n^{(1)}(k_{i_\rho}\rho')R_{i,i-1}(1,1)\right]\\
&+\left\{J_n(k_{i_\rho}\rho)R_{i,i+1}(2,1)M_i(1,2)\right.\\
&\left.+\left[H_n^{(1)}(k_{i_\rho}\rho)+J_n(k_{i_\rho}\rho)R_{i,i+1}(2,2)\right]M_i(2,2)\right\}\\
&\cdot H_n^{(1)}(k_{i_\rho}\rho')R_{i,i-1}(2,1) \qquad (25c)\\
f_{22} &= \left\{J_n(k_{i_\rho}\rho)R_{i,i+1}(2,1)M_i(1,1)\right.\\
&\left.+\left[H_n^{(1)}(k_{i_\rho}\rho)+J_n(k_{i_\rho}\rho)R_{i,i+1}(2,2)\right]M_i(2,1)\right\}\\
&\cdot H_n^{(1)}(k_{i_\rho}\rho')R_{i,i-1}(2,1)+\left\{J_n(k_{i_\rho}\rho)R_{i,i+1}(2,1)M_i(1,2)\right.\\
&\left.+\left[H_n^{(1)}(k_{i_\rho}\rho)+J_n(k_{i_\rho}\rho)R_{i,i+1}(2,2)\right]M_i(2,2)\right\}\\
&\cdot\left[J_n(k_{i_\rho}\rho')+H_n^{(1)}(k_{i_\rho}\rho')R_{i,i-1}(2,2)\right]\\
&-H_n^{(1)}(k_{i_\rho}\rho')J_n(k_{i_\rho}\rho')+H_n^{(1)}(k_{i_\rho}\rho)J_n(k_{i_\rho}\rho')\\
&= f'_{22}+H_n^{(1)}(k_{i_\rho}\rho)J_n(k_{i_\rho}\rho'). \qquad (25d)
\end{aligned}
$$

After the spectral domain mixed potential Green's function is calculated accurately, the DCIM and GPOF technique are used to yield the mixed potential spatial domain Green's function in fast computational form. Details will be discussed in the next section.

3. NUMERICAL RESULTS AND DISCUSSION

In order to verify the proposed procedure, a multilayered cylindrical structure shown in Fig. 3 is investigated. The source and observation points are located at $\rho = \rho' = 51$ mm and $\phi - \phi' = 0.5236$, respectively. For the deformed Sommerfeld integral path (SIP) parameters, we choose $T_1 = 0.1$, $T_2 = 3.0$, and $T_3 = 23.5$. The spectral domain Green's function is sampled uniformly along the deformed SIP described by

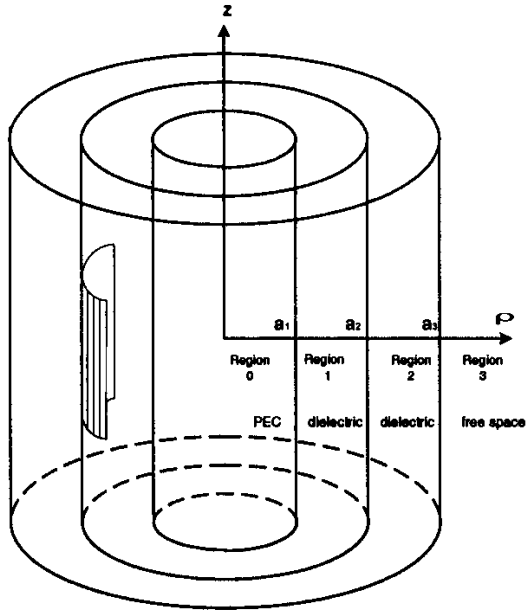

Figure 3. Dielectric-coated conducting cylinder with a superstrate where the shaded area denotes a patch located on the interface between region 1 and region 2. Parameters used are $a_1 = 48\,\text{mm}$, $a_2 = 51\,\text{mm}$, $a_3 = 54\,\text{mm}$, $\mu_{r_1} = \mu_{r_2} = \mu_{r_3} = 1$, $\epsilon_{r_1} = 2.3$, $\epsilon_{r_2} = 5.8$, $\epsilon_{r_3} = 1$, $f = 6.8\,\text{GHz}$, $\rho = \rho' = 51\,\text{mm}$, and $\phi - \phi' = 0.5236$.

following equations similar to that in [14]

$$k_z = k_s(1 - jT_1)\frac{t_1}{T_1}, \quad \text{for } \Gamma_1;$$

$$k_z = k_s\left[1 - jT_1 + \left(\sqrt{1 + T_2^2} - 1 + jT_1\right)\frac{t_2}{T_2 - T_1}\right], \quad \text{for } \Gamma_2;$$

$$k_z = k_s\sqrt{1 + (t_3 + T_2)^2}, \quad \text{for } \Gamma_3;$$

where $0 \le t_1 < T_1$, $0 \le t_2 < T_2 - T_1$, $0 \le t_3 < T_3 - T_2$, and k_s represents the wavenumber of the sampling region that is chosen as the source layer. The above three equations correspond to paths Γ_1, Γ_2 and Γ_3, respectively. The parameters T_2 and T_3 must be chosen to be large enough to enable the large argument approximation of the zero order Hankel functions to be valid. The deformed path can be neither too close to nor too far away from the real axis in k_z complex plane, the appropriate value of T_1 can range from 0.05 to 0.5. The complex images

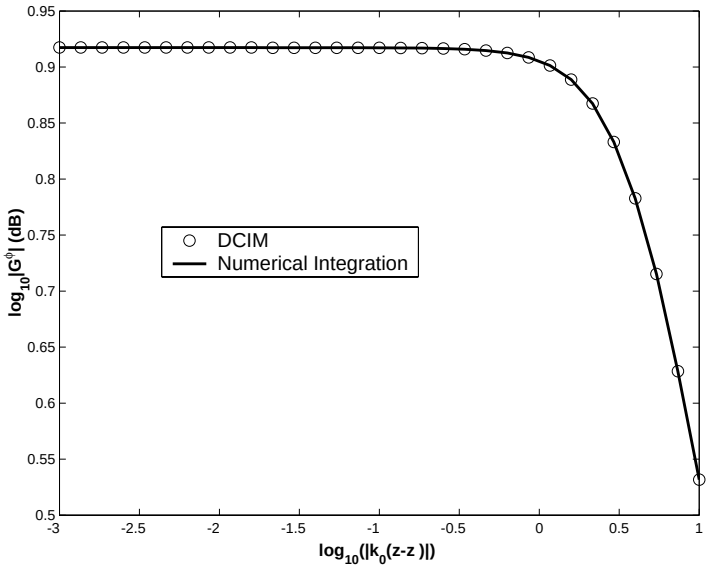

Figure 4. Magnitude of spatial domain Green's function G^{ϕ} for the structure shown in Fig. 3.

in each segment are chosen as 5 for the segment $0 \leq t_1 < T_1$, 5 for the segment $0 \leq t_2 < T_2 - T_1$, and 2 for the segment $0 \leq t_3 < T_3 - T_2$, respectively. The sampling points in each segment of the paths are: 100 points for path Γ_1, 100 points for path Γ_2, and 100 points for the remaining path, correspondingly.

After subtractions of $[H_n^{(1)}(k_{i_\rho}\rho)J_n(k_{i_\rho}\rho')]$ from f_{11} and f_{22}, we perform the summation of cylindrical harmonics in (19), (20a) and (20b) with the help of Shank's transform [21]. Good convergent results can be obtained for summation up to 200 harmonics. The choice of 200 is made for the robust consideration of the program. After the summation of the cylindrical harmonics is convergently achieved, we perform the DCIM or the two step GPOF method [14] to carry out the Sommerfeld integral. By making use of cylindrical coordinate Sommerfeld identity, the $[H_n^{(1)}(k_{i_\rho}\rho)J_n(k_{i_\rho}\rho')]$ subtracted in spectral domain Green's function can be transformed to spatial domain in closed form.

In this paper, spatial domain mixed potential Green's functions are calculated using the fore-mentioned numerical technique. It costs 3.9 seconds per angle for computing all the necessary mixed potential Green's functions as shown in Figs. 4–6 on a Pentium-III 800 PC (the

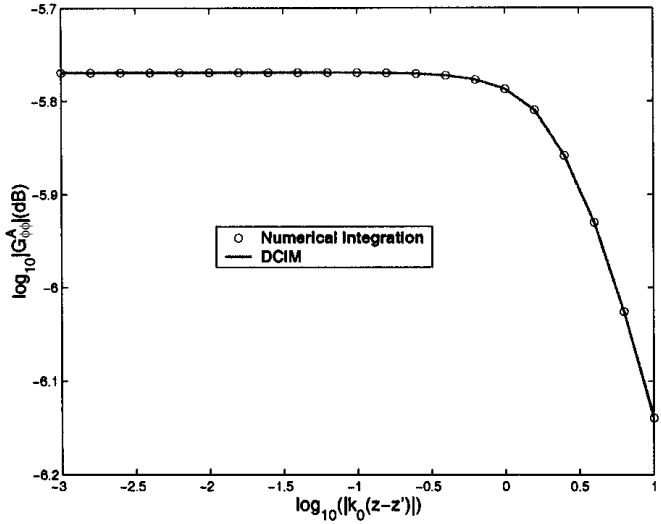

Figure 5. Magnitude of spatial domain Green's function $G^A_{\phi\phi}$ for the structure shown in Fig. 3.

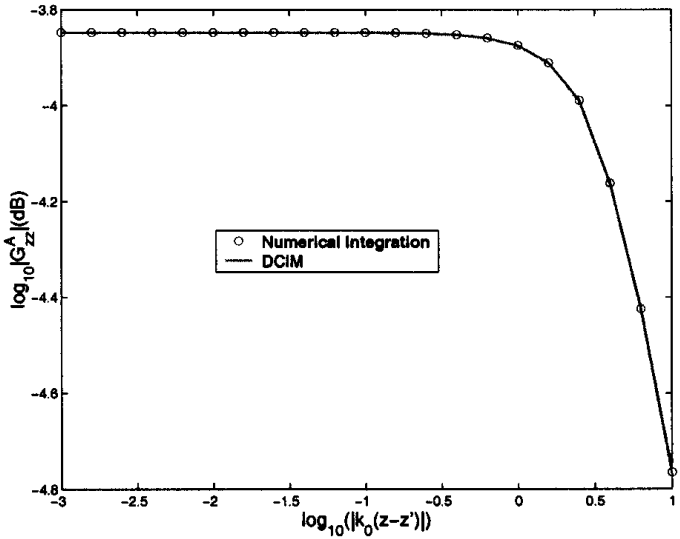

Figure 6. Magnitude of spatial domain Green's function G^A_{zz} for the structure shown in Fig. 3.

convergence accuracy for the spatial domain Green's functions is set to be 10^{-3}). Figures 5 and 6 depict two components of the vector potential Green's functions, and Figure 4 shows the scalar potential Green's function. Approximate Green's functions are computed and compared with the exact Green's functions obtained by the direct numerical integrals, and they are in a good agreement. For very small $(\phi - \phi')$ (i.e., $\phi - \phi' < 0.05$), however, we find that a large number of harmonics is needed for achieving the convergence of the summation.

4. CONCLUSION

Different from the previous work, the present paper derived theoretically and obtained numerically the mixed potential Green's functions for cylindrically multilayered media in spatial domain. The magnetic vector potential and scalar potential Green's function are derived by decomposing the electric field Green's functions into a suitable form. After $[H_n^{(1)}(k_{i_\rho}\rho)J_n(k_{i_\rho}\rho')]$ is subtracted from the Green's functions, the remaining part is summed up with the help of Shank's transform and integrated with the help of GPOF method. The subtracted term is transformed into the spatial domain in closed form by using the Sommerfeld identity. Numerical results show that the procedure for fast computation of spatial domain mixed potential Green's functions for cylindrically multilayered media is applicable and reliable.

REFERENCES

1. Fang, D. G., J. J. Yang, and G. Y. Delisle, "Discrete image theory for horizontal electric dipole in a multilayer medium," *Proc. Inst. Elect. Eng. H*, Vol. 135, 297–303, Oct. 1988.
2. Chow, Y. L., J. J. Yang, D. G. Fang, and G. E. Howard, "A closed-form spatial Green's function for the thick microstrip substrate," *IEEE Trans. Microwave Theory Tech.*, Vol. 39, 558–592, Mar. 1991.
3. Yang, J. J., Y. L. Chow, G. E. Howard, and D. G. Fang, "Complex images of an electric dipole in homogeneous and layered dielectrics between two grounded planes," *IEEE Trans. Microwave Theory Tech.*, Vol. 40, 595–600, Mar. 1992.
4. Tai, C. T., *Dyadic Green's Functions in Electromagnetic Theory*, 2nd ed., IEEE Press, Piscataway, NI, 1994.
5. Kipp, R. A. and C. H. Chan, "Complex image method for

sources in bounded regions of multilayer structures," *IEEE Trans. Microwave Theory Tech.*, Vol. 42, 860–865, May 1994.

6. Aksun, M. I. and R. Mittra, "Derivation of closed-form spatial Green's functions for a general microstrip geometry," *IEEE Trans. Microwave Theory Tech.*, Vol. 40, 2055–2062, Nov. 1992.
7. Dural, G. and M. I. Aksun, "Closed-form Green's functions for general sources and stratified media," *IEEE Trans. Microwave Theory Tech.*, Vol. 43, 1545–1552, July 1995.
8. Aksun, M. I., "A robust approach for the derivation of closed-form spatial Green's functions," *IEEE Trans. Microwave Theory Tech.*, Vol. 44, 651–658, May 1996.
9. Ling, F. and J. M. Jin, "Discrete complex image method for Green's functions of general multilayer media," *IEEE Microwave Guided Wave Lett.*, Vol. 10, 400–402, Oct. 2000.
10. Chew, W. C., *Waves and Fields in Inhomogeneous Media*, Van Nostrand Reinhold, New York, 1990.
11. Li, L. W., M. S. Leong, T. S. Yeo, and P. S. Kooi, "Electromagnetic dyadic Green's functions in spectral domain for multilayered cylinders," *J. Electromagn. Waves and Appl.*, Vol. 14, 961–986, Jul. 2000.
12. Donohoe, J. P., "Scattering from buried bodies of revolution using dyadic Green's functions in cylindrical harmonics," *IEEE Antennas Propagat. Soc. Int. Symp. Dig.*, Vol. 4, 1922–1925, Atlanta, GA, June 1998.
13. Thiel, M. and A. Dreher, "Dyadic Green's function of multilayer cylindrical closed and sector structures for waveguide, microstrip-antenna and network analysis," *IEEE Trans. Microwave Theory Tech.*, Vol. 50, 2576–2579, Nov. 2002.
14. Tokgöz, C. and G. Dural, "Closed-form Green's functions for cylindrically stratified media," *IEEE Trans. Microwave Theory Tech.*, Vol. 48, 40-49, Jan. 2000.
15. Sun, J., C. F. Wang, L. W. Li, and M. S. Leong, "A complete set of spatial-domain dyadic Green's function components for cylindrically stratified media in fast computational form," *J. Electromagn. Waves and Appl.*, Vol. 16, No. 11, 1491–1509, 2002.
16. Hua, Y. and T. K. Sarkar, "Generalized pencil-of-function method for extracting poles of an EM system from its transient response," *IEEE Trans. Antennas Propagat.*, Vol. 37, 229–234, Feb. 1989.
17. Ertürk, V. B. and R. G. Rojas, "Efficient computation of surface fields excited on a dielectric-coated circular cylinder," *IEEE Trans. Antennas Propagat.*, Vol. 48, No. 10, 1507–1516, Oct. 2000.

18. Svezhentsev, A. and G. Vandenbosch, "Model for the analysis of microstrip cylindrical antennas: efficient calculation of the necessary Green's functions," *11th Int. Conf. Antennas Propagat.*, Vol. 2, 615–618, Manchester, UK, Apr. 2001.
19. Hall, R. C., C. H. Thng, and D. C. Chang, "Mixed potential Green's functions for cylindrical microstrip structures," *IEEE Antennas Prapagat. Soc. Int. Symp.*, Vol. 4, 1776–1779, 1995.
20. Chen, J., A. A. Kishk, and A. W. Glission, "Application of a new mpie formulation to the analysis of a dielectric resonator embedded in a multilayered medium couple to a microstrip circuit," *IEEE Trans. Microwave Theory Tech.*, Vol. 49, No. 2, 263–279, Feb. 2001.
21. Shank, D., "Non-linear transformation of divergent and slowly convergent sequences," *J. Math. Phy.*, Vol. 34, 1–42, 1955.

Jin Sun received the degrees of B.Sc. in Physics and M.Eng.Sc. in Electrical Engineering from Wuhan University, Wuhan, China, in 1992 and 1995, respectively. He is currently with the Department of Electrical and Computer Engineering at the National University of Singapore, where he is a Research Scholar toward his Ph.D. degree. His main research interests include integral equation methods, fast algorithms, and discrete complex image method.

Chao-Fu Wang received the B.Sc. degree in mathematics from the Henan Normal University, Xinxiang, China, in 1985, the M.Sc. degree in applied mathematics from the Hunan University, Changsha, China, in 1989, and the Ph.D. degree in electrical engineering from the University of Electronic Science and Technology of China, Chengdu, China, in 1995, respectively. From 1987 to 1996, he was a Lecturer, and then an Associate Professor of the Department of Applied Mathematics at the Nanjing University of Science and Technology (NUST). Since February 1996, he has been an Associate Professor of the Department of Electronic Engineering at the NUST. From 1996–1999, he was a Postdoctoral Research Fellow in the Center for Computational Electromagnetics (CCEM), University of Illinois at Urbana-Champaign (UIUC). From 1999–2001, he was a Research Fellow in the Department of Electrical and Computer Engineering, National University of Singapore (NUS). He is currently a Research Scientist and Project Leader in the Temasek Laboratories, NUS. His current research interests include fast algorithms for computational electromagnetics, scattering and antenna analysis, ferrite components and their analysis, MMIC design and fast EM simulation.

Le-Wei Li received the degrees of B.Sc. in Physics, M.Eng.Sc. and Ph.D. in Electrical Engineering from Xuzhou Normal University, Xuzhou, China, in 1984, China Research Institute of Radiowave Propagation (CRIRP), Xinxiang, China, in 1987 and Monash University, Mel bourne, Australia, in 1992, respectively. In 1992, he worked at La Trobe University (jointly with Monash University), Melbourne, Australia as a Research Fellow. Since 1992, He has been with the Department of Electrical Engineering at the National University of Singapore where he is currently a Professor. Since 1999, he has been also part-timely with High Performance Computation of Engineered Systems (HPCES) Programme of Singapore-MIT Alliance (SMA) as a SMA Fellow. His current research interests include electromagnetic theory, radio wave propagation and scattering in various media, microwave propagation and scattering in tropical environment, and analysis and design of antennas. In these areas, he, as the principal author of a book entitled *Spheroidal Wave Functions in Electromagnetic Theory* by John Wiley in 2001, has published 31 book chapters, over 180 international refereed journal papers, 25 regional refereed journal papers, and over 190 international conference papers. He serves as an Associate Editor of *Journal of Electromagnetic Waves and Applications* and *Radio Science*, an Editorial Board Member of *IEEE Transactions on Microwave Theory and Techniques, Electromagnetics* journal, and an Overseas Editorial Board Member of *Chinese Journal of Radio Science*.

Mook-Seng Leong received the B.Sc. degree in electrical engineering (with first class honors) and the Ph.D. degree in microwave engineering from the University of London, England, in 1968 and 1971, respectively. He is currently a Professor of Electrical Engineering at the National University of Singapore. His main research interests include antenna and waveguide boundary-value problems. Dr. Leong is a member of the MIT-based Electromagnetic Academy and a Fellow of the Institution of Electrical Engineers, London. He received the 1996 Defence Science Organization (DSO) R&D Award from DSO National Laboratories, Singapore in 1996. He is a member of the Editorial Board for Microwave and Optical Technology Letters and Wireless Mobile Communications.